

Hysteresis effects in the phase diagram of multiferroic GdMnO₃

J. Baier,¹ D. Meier,¹ K. Berggold,¹ J. Hemberger,² A. Balbashov,³ J. A. Mydosh,¹ and T. Lorenz^{1*}

¹*II. Physikalisches Institut, University of Cologne, Germany*

²*Institut für Physik, University of Augsburg, Germany*

³*Moscow Power Engineering Institute, Moscow, Russia*

(Dated: December 28, 2021)

We present high-resolution thermal expansion $\alpha(T)$ and magnetostriction $\Delta L(H)/L$ measurements of GdMnO₃, which develops an incommensurate antiferromagnetic order (ICAFM) below $T_N \simeq 42$ K and transforms into a canted A-type antiferromagnet (cAFM) below $T_c \simeq 20$ K. In addition, a ferroelectric polarization $\mathbf{P}||a$ is observed below T_{FE} for finite magnetic fields applied along the b direction. In zero magnetic field we find a strongly anisotropic thermal expansion with certain, rather broad anomalous features. In finite magnetic fields, however, very strong anomalies arise at T_c for fields applied along each of the orthorhombic axes and at T_{FE} for fields along the b axis. Both phase transitions are of first-order type and strongly hysteretic. We observe a down-bending of the ICAFM-to-cAFM phase boundary $T_c(H)$ for low magnetic fields and our data give evidence for coexisting phases in the low-field low-temperature range.

The recent discovery of very large magnetoelectric effects in the rare-earth manganites $RMnO_3$ has reopened the field of the so-called multiferroic materials.^{1,2} Multiferroic means, that several ferro-type orders like ferromagnetism, ferroelectricity or ferroelasticity coexist. The rare-earth manganites $RMnO_3$ may be grouped into the hexagonal ones ($R = \text{Ho}, \dots, \text{Lu}$) and those with orthorhombically distorted perovskite structures ($R = \text{La}, \dots, \text{Dy}$). The hexagonal $RMnO_3$ show both, ferroelectric and magnetic order, but the respective ordering temperatures differ by an order of magnitude, $T_{FE} \simeq 1000$ K and $T_N \simeq 100$ K.³ In contrast, $RMnO_3$ with $R = \text{Gd}, \text{Tb}$, and Dy possess comparable transition temperatures for the magnetic and the ferroelectric ordering.^{1,2} Both, TbMnO_3 and DyMnO_3 develop an incommensurate antiferromagnetic order (ICAFM) below about 40 K. The incommensurability continuously changes upon cooling and becomes almost constant below $T_c \simeq 28$ K and $\simeq 19$ K for $R = \text{Tb}$ and Dy , respectively. The transition to this long-wavelength incommensurate antiferromagnetic (LT-ICAFM) phase is accompanied by ferroelectric (FE) ordering with a polarization $\mathbf{P}||c$, which flops to $\mathbf{P}||a$ above a critical magnetic field applied along the a or b direction, while it is suppressed for large fields along c .⁴ GdMnO₃ also shows an ICAFM order below $T_N \simeq 42$ K and a second transition at $T_c \simeq 23$ K. Based on the observed weak ferromagnetism^{5,6} and on X-ray diffraction studies⁷ a canted A-type antiferromagnetic ordering (cAFM) has been proposed for $T < T_c$, but a direct magnetic structure determination has not yet been published. Both transition temperatures weakly increase in a magnetic field.⁴ Concerning the FE polarization, contradictory results have been reported. Kuwahara *et al.*⁸ find a finite polarization below 13 K, while Kimura *et al.*⁴ observe FE order only between 5 K and 8 K. The magnitude of \mathbf{P} is much smaller than in TbMnO_3 and DyMnO_3 and the direction is $\mathbf{P}||a$. Moreover, there are no magnetic-field-induced polarization flops. Instead the polarization is stabilized by a magnetic field along b , while it is immediately suppressed for fields along a and c .^{4,8}

In order to study the coupling of the various phase boundaries to lattice degrees of freedom we have conducted high-resolution measurements of thermal expansion and magnetostriction on GdMnO₃. We find pronounced anomalies at all transitions, i.e. all transitions strongly couple to the lattice. Thus, our data allow for a precise determination of the magnetic-field temperature phase diagram and clearly reveal that the ICAFM-to-cAFM as well as the FE transition are of first order with strong hysteresis. For low magnetic fields we find a down-bending of the ICAFM-to-cAFM phase boundary and evidence for a coexistence of both phases in this low-field range. This should be taken into account for further experiments, in particular for zero magnetic field. Probably, this may also explain the contradictory results reported for GdMnO₃.^{4,8,9}

The GdMnO₃ single crystal used in this study is a cuboid of dimensions $1.7 \times 2 \times 1.45$ mm³ along the a , b , and c direction ($Pbnm$ setting), respectively. It was cut from a larger crystal grown by floating-zone melting. Phase purity was checked by x-ray powder diffraction.¹⁰ Magnetization, resistivity and specific heat data of the same crystal are reported in Ref. 6. The linear thermal expansion $\alpha_i = \partial \ln L_i / \partial T$ and magnetostriction $\Delta L_i(H)/L_i = [L_i(H) - L_i(0)]/L_i(0)$ have been measured by a home-built high-resolution capacitance dilatometer.¹¹ Here, L_i denote the lengths parallel to the different crystal axes $i = a, b$, and c . In general, we studied the length changes in longitudinal magnetic fields up to 14 T, i.e. $H||i$, and, in addition, we measured α_b for $H||c$.

Fig. 1 shows the zero-field α_i of GdMnO₃ for $i = a, b$, and c , which are strongly anisotropic and show several anomalies. The sharp anomalies around 41 K signal the Néel transition of the Mn ions and their shape is typical for a second-order phase transition. According to previous publications further anomalies are expected at lower T : (i) at the ICAFM-to-cAFM transition around $T_c \simeq 23$ K, (ii) around $T_{FE} \simeq 10$ K, where the FE ordering sets in, and (iii) around 6 K due to the ordering of the Gd moments. Indeed, there are pronounced anoma-

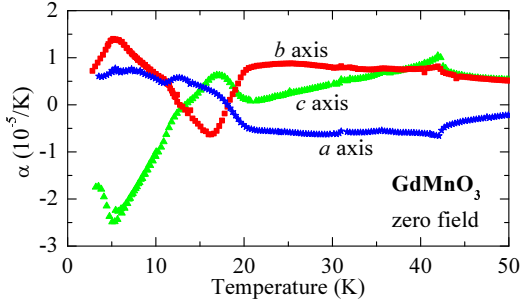


FIG. 1: (Color online) Thermal expansion of GdMnO_3 along a , b , and c .

lies around 6 K, small ones around 10 K, and intermediate ones around 20 K with different signs and magnitudes for the different i . However, all these anomalies are rather broad making a clear identification of transition temperatures difficult. This drastically changes for finite magnetic fields.

In Fig. 2 we show $\alpha_a(T)$ for $H||a$. With increasing magnetic field a broad anomaly shows up around 10 K, changes sign and smears out above 2 T. The origin of this anomaly is unclear, it may be related to the complex interplay of the magnetism of the Mn and Gd ions.⁶ The most drastic change occurs, however, around 18 K, where a huge anomaly emerges between 0 and 1 T. This anomaly is close to the observed ICAFM-to-cAFM transition at T_c and systematically shifts to higher T with further increasing field, in agreement with the observed field dependence $T_c(H)$.^{1,4,7} The negative sign of the anomaly means that the transition from the cAFM to the ICAFM phase, with increasing T , is accompanied by a pronounced contraction of the a axis (see also Fig. 3). The $\alpha_a(T)$ curves of Fig. 2a have been recorded with increasing T in the so-called field-cooled (FC) mode, i.e. the field has been applied at $T \simeq 50$ K. We have also recorded the data during the cooling runs. Fig. 2b compares $\alpha_a(T)$ obtained with increasing and decreasing T for $H = 4$ T. Obviously, there is a strong hysteresis at the ICAFM-to-cAFM transition identifying this transition as first-order type.

The lower panels of Fig. 2 present the magnetostriction $\Delta L_a(H)/L_a$ for $H||a$ at constant T . At 20 K an anomalous expansion of the a axis occurs around 4 T, which is related to a transition from the ICAFM to the cAFM phase as a function of increasing H . Both, the position of the $\Delta L_a(H)/L_a$ anomaly in the $H - T$ plane and its magnitude fit to the position and magnitude of the corresponding $\alpha_a(T)$ anomaly due to the ICAFM-to-cAFM transition as a function of decreasing T . The $\Delta L_a(H)/L_a$ curves obtained with increasing and decreasing H also show a hysteresis at the ICAFM-to-cAFM transition. With decreasing T the anomaly of $\Delta L_a(H)/L_a$ shifts towards lower field. Around 12 K an anomalous expansion of the a axis is observed with increasing H , however, this expansion is not reversed upon decreasing the field. Due to the large hysteresis GdMnO_3 remains in

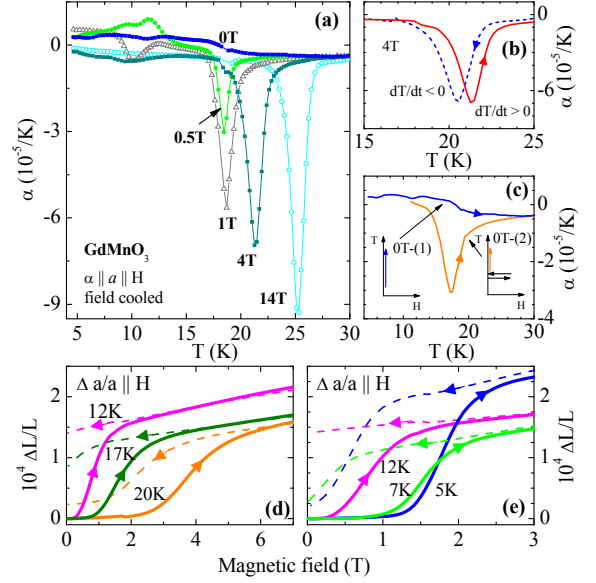


FIG. 2: (Color online) Panel (a): Field-cooled thermal expansion $\alpha_a(T)$ for $H||a$ measured with increasing T . Panel (b) shows the hysteresis around T_c between the data obtained with increasing and decreasing T . Panel (c) compares two zero-field $\alpha_a(T)$ curves for increasing T . The first curve [0T-(1)] has been recorded after zero-field cooling the sample and the second [0T-(2)] after cooling the sample to 12 K and subsequently applying and removing a magnetic field of 8 T. The lower panels (d) and (e) present the zero-field cooled magnetostriction $\Delta L_i(H)/L_i$ recorded with increasing (solid lines) and decreasing (dashed) field.

the cAFM phase after the magnetic field is switched off. With further decreasing T , the anomaly of $\Delta L_a(H)/L_a$ again shifts to higher field and at 5 K the anomalous expansion occurring with increasing H is reversed again with decreasing field. Apparently, we have traced the field-induced transition to the cAFM phase down to our lowest T . This means that the ICAFM-to-cAFM phase boundary $T_c(H)$ shows a clear down-bending in the low-field range (see Fig. 5). In order to verify this, we have carried out the following zero-field $\alpha_a(T)$ measurement: after cooling the sample to 12 K in zero field we have applied a magnetic field of 8 T in order to enter the cAFM phase and due to the hysteresis of the ICAFM-to-cAFM transition the sample should remain in the cAFM phase after removing the field again. Fig. 2c shows a comparison of this zero-field $\alpha_a(T)$ [labeled as 0T-(2)] with the conventional FC $\alpha_a(T)$ [0T-(1)]. In contrast to the 0T-(1) curve, the 0T-(2) measurement shows a sharp peak around T_c , which is comparable to the anomaly of the finite-field $\alpha_a(T)$ curves. This clearly confirms the down bending of the ICAFM-to-cAFM phase boundary. Thus, the (pure) cAFM phase of GdMnO_3 cannot be reached by cooling the crystal in zero field. The broad anomalies in the zero-field $\alpha_i(T)$ curves (see Fig. 1) probably arise from a partial ICAFM-to-cAFM transition and suggest that both phases coexist in the low-field region.

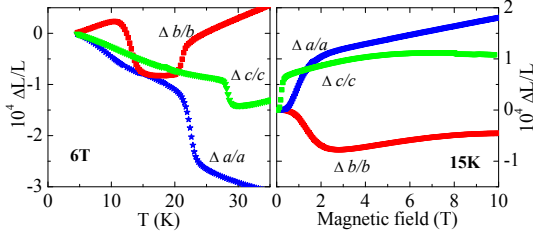


FIG. 3: (Color online) The relative length changes of the a , b , and c axes as a function of T at constant field ($H = 6$ T; left) and as a function of H at constant temperature ($T = 15$ K; right). In all cases H was applied parallel to the measured direction.

In Fig. 3 we compare the relative length changes as a function of field and temperature for all three axes. The c axis behaves similar to the a axis. The anomalies of c have the same signs but smaller magnitudes as compared to those of a and, moreover, their position for the same field (temperature) is located at higher T (lower H). Since in all cases we applied $H \parallel L_i$, the latter difference signals the anisotropy with respect to the field direction. Our results (not shown) for $\alpha_c(T)$ and $\Delta L_c(H)/L_c$ for other fields and temperatures, respectively, are very similar to those obtained for the a axis. In particular, the distinct expansion at the ICAFM-to-cAFM transition as a function of field or temperature is only present for $H \gtrsim 0.2$ T. The hysteresis is also strong for $H \parallel c$, but less pronounced than for $H \parallel a$ (see Fig. 5). A different phenomenology is observed for $\Delta L_b/L_b$ for $H \parallel b$. Firstly, the anomalies at the ICAFM-to-cAFM transition are of opposite signs and, secondly, an additional anomaly occurs at a lower temperature.

In Fig. 4 we present $\alpha_b(T)$ for different $H \parallel b$. Again, a very pronounced anomaly evolves around $T_c \simeq 18$ K in small fields and shifts to higher T with further increasing field. The behavior of α_b is analogous to our results on α_a and α_c , only the signs of the anomalies are different. In contrast to α_a and α_c , however, an additional, very pronounced anomaly develops around 12 K in finite fields. Based on the polarization data of Ref. 4, we attribute this anomaly to the FE ordering at T_{FE} . As a further verification we have also measured α_b in a transverse magnetic field $H \parallel c$ and did not find such an additional anomaly (see inset of Fig. 4a). As shown in the lower inset of Fig. 4b the transition to the FE phase is also of first-order type with a broad hysteresis. With further increase of the magnetic field above 8 T the magnitude of the T_{FE} anomaly decreases again and vanishes around 12 T. This disappearance is a consequence of the strong hysteresis of the FE transition and occurs only in the FC measurements of α_b . The upper inset of Fig. 4b compares the FC and zero-field-cooled (ZFC) measurements of α_b for $H = 12$ T $\parallel b$. The ZFC curve displays a large anomaly at T_{FE} , which is absent in the FC curve. This difference arises from a decreasing $T_{FE}(H)$ with increasing field. When the lower $T_{FE}(H)$ is smaller than

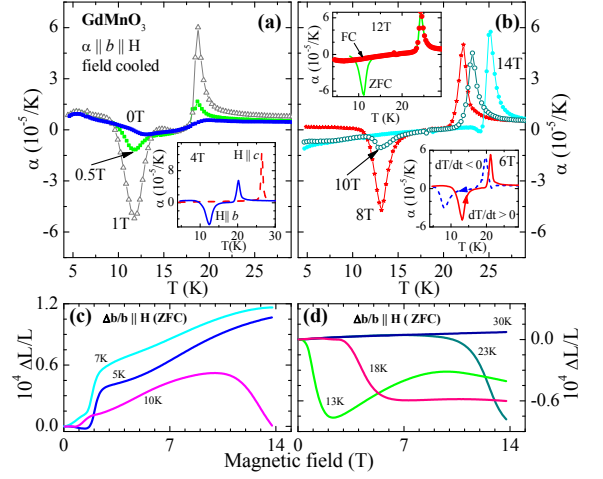


FIG. 4: (Color online) Field-cooled measurements of $\alpha_b(T)$ in fields up to 1 T (a) and between 8 T and 14 T (b). The inset of panel (a) compares $\alpha_b(T)$ for $H = 4$ T applied along b (solid line) and c (dashed). The upper inset of panel (b) shows $\alpha_b(T)$ for $H = 12$ T ($H \parallel b$; $dT/dt > 0$) obtained in a FC (symbols) and a ZFC run (line). The lower inset displays the hysteresis between $\alpha_b(T)$ for $H = 6$ T recorded with $dT/dt > 0$ (solid line) and $dT/dt < 0$ (dashed). Panels (c) and (d) show the ZFC magnetostriction obtained for $dH/dt > 0$.

our lowest measurement temperature of $\simeq 4.5$ K the FE phase cannot be reached in a FC run and, consequently, there is no anomaly in the subsequent $\alpha_b(T)$ measured with increasing T . The FE phase can, however, be entered by cooling the sample in a lower field, e.g. 6 T (see lower inset of Fig. 4b), or in a ZFC run when the field is applied at the lowest temperature. Due to the large hysteresis the sample remains in the FE phase up to high fields and therefore the ZFC $\alpha_b(T)$ curves show anomalies at the upper $T_{FE}(H)$ when the FE phase is left upon heating.

The lower panels (c) and (d) of Fig. 4 show the magnetostriction. In agreement with the negative signs of the α_b anomalies we observe a pronounced contraction at the field-induced ICAFM-to-cAFM transition for $T \gtrsim 13$ K. At lower T we still find clear anomalies, however, of opposite sign. This sign change results from the fact that below about 10 K the FE phase is entered, which has a significantly longer b axis than both, the cAFM phase and a low- T extrapolation of the ICAFM phase (see Fig. 3). The strong decrease of $\Delta b/b$ at 10 K for $H \gtrsim 10$ T signals a field-induced FE-to-cAFM transition due to the above-mentioned negative slope of the $T_{FE}(H)$ boundary.

Based on our measurements of α_i and $\Delta L_i(H)/L_i$ with $H \parallel i$ for all three crystallographic axes i we derive the phase diagrams presented in Fig. 5. The weak field dependence of $T_N \simeq 42$ K well agrees with previous results.⁴ The new feature of our phase diagram is the down-bending of the ICAFM-to-cAFM phase boundary at low magnetic field. This transition exhibits a strong hysteresis and we conclude that the ICAFM and the cAFM

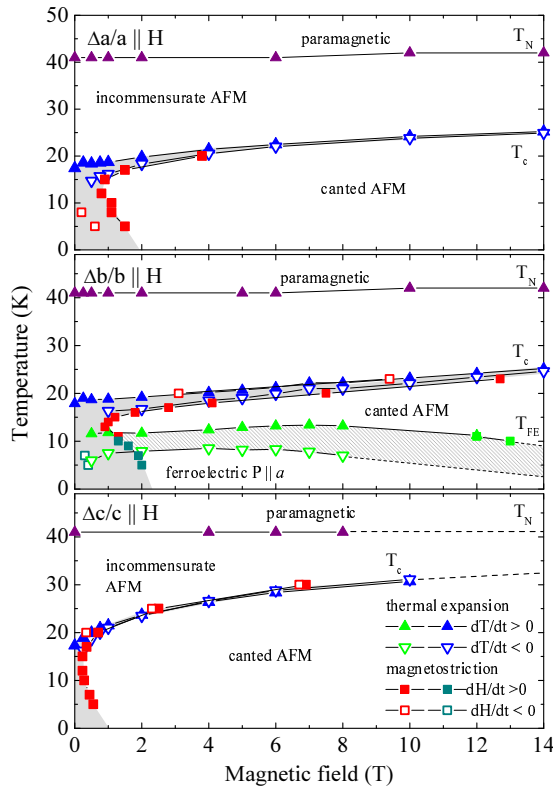


FIG. 5: (Color online) Phase diagrams of GdMnO₃ based on the measurements of α_i (triangles) and $\Delta L_i(H)/L_i$ (squares) measured along $i = a, b$, and c with $H \parallel i$. Filled and open symbols are obtained with increasing and decreasing T or H , respectively. Hatched areas signal regions of strong hysteresis, where different phases coexist.

phases coexist in the low-field low-temperature region. Such a coexistence can naturally explain why the zero-field $\alpha_i(T)$ curves only show some broad anomalous features around 18 K instead of the distinct anomalies which signal the transition from the cAFM to the ICAFM phase for larger fields. This conclusion is also supported by measurements of the polarization showing that the magnitude of \mathbf{P} in this hysteretic region is much smaller than both, \mathbf{P} for larger $H \parallel b$ and \mathbf{P} of $RMnO_3$ with $R = Tb$ and Dy .⁴

As shown in Fig. 4a the magnitudes of the α_b anomalies at T_{FE} and T_c simultaneously evolve between 0 and 1 T. This correlation suggests that the ICAFM-to-cAFM

transition is a precondition for the FE ordering. As mentioned above the notation 'cAFM' should be treated with some caution, because the magnetic structure of GdMnO₃ has not yet been unambiguously determined. In a simplified picture, the proposed structure can be described as follows: the Mn moments are oriented approximately along b with some canting towards c , along the a (c) direction neighboring moments are essentially parallel (antiparallel) with respect to each other, and along b an incommensurate modulation of the moments is present above and vanishes below T_c . This view is supported by the phase diagram, since the stabilization of the cAFM phase is most pronounced for $H \parallel c$ as it is expected for a cAFM phase with a weak ferromagnetic moment pointing along c already in zero field. A field along a also points approximately perpendicular to the Mn moments, and one can therefore expect that the Mn moments (and also the weak ferromagnetic moment) are slightly canted towards a . However, a more drastic change is expected for $H \parallel b$, since 50% of the Mn moments are oriented roughly antiparallel to H . In simple antiferromagnets this configuration usually leads to a spin-flop transition, i.e. the Mn moment would jump to the ac plane and cant towards b . Such a configuration would be analogous to those for $H \parallel a$ or c and according to Ref. 12 none of these configurations would lead to a finite polarization via a coupling of the magnetic and ferroelectric order parameters. However, in view of the more complex magnetic structures observed in neighboring $RMnO_3$, one may speculate that a similar complex structure could be induced in GdMnO₃ for $H \parallel b$, and this might explain the finite FE polarization via a coupling between AFM and FE order parameters.^{12,13} Hence, there is need for a detailed determination of the magnetic structure of GdMnO₃.

In summary, we have presented a study of the magnetic-field temperature phase diagram of GdMnO₃ via thermal expansion and magnetostriction measurements. We find that both, the ICAFM-to-cAFM as well as the FE transition are of first-order type and strongly hysteretic. The hysteresis is most pronounced in the low-field range. We find a down-bending of the ICAFM-to-cAFM phase boundary and evidence for coexisting ICAFM and cAFM phases in this low-field range.

We acknowledge fruitful discussions with D. Khomskii. This work was supported by the Deutsche Forschungsgemeinschaft through SFB 608. JAM is supported by the Alexander von Humboldt Stiftung.

* Electronic address: lorenz@ph2.uni-koeln.de

¹ T. Kimura *et al.*, Nature **426**, 55 (2003).

² T. Goto *et al.*, Phys. Rev. Lett. **92**, 257201 (2004).

³ M. Fiebig *et al.*, Nature **419**, 818 (2002).

⁴ T. Kimura *et al.*, Phys. Rev. B **71**, 224425 (2005).

⁵ T. Kimura *et al.*, Phys. Rev. B **68**, 060403(R) (2003).

⁶ J. Hemberger *et al.*, Phys. Rev. B **70**, 024414 (2004).

⁷ T. Arima *et al.*, Phys. Rev. B **72**, 100102(R) (2005).

⁸ H. Kuwahara *et al.*, Physica B **359**, 1279 (2005).

⁹ According to Ref. 14 this discrepancy could also arise from weak oxygen off-stoichiometries in different crystals.

¹⁰ A. Kadomtseva *et al.*, Sov. Phys. JETP Lett. **81**, 22 (2005).

¹¹ T. Lorenz *et al.*, Phys. Rev. B **55**, 5914 (1997).

¹² M. Mostovoy, Phys. Rev. Lett. **96**, 067601 (2006).

¹³ M. Kenzelmann *et al.*, Phys. Rev. Lett. **95**, 087206 (2005).

¹⁴ T. Goto *et al.*, Phys. Rev. B **72**, 220403(R) (2005).